JACS
JOURNAL OF THE AMERICAN CHEMICAL SOCIETY
Communication
pubs.acs.org/JACS

Carbon Monoxide-Assisted Size Confinement of Bimetallic Alloy Nanoparticles

Chunhua Cui,[†] Lin Gan,[†] Maximilian Neumann,[†] Marc Heggen,[‡] Beatriz Roldan Cuenya,[§] and Peter Strasser*,[†]

[†]The Electrochemical Energy, Catalysis, and Materials Science Laboratory, Department of Chemistry, Chemical Engineering Division, Technical University Berlin, Berlin 10623, Germany

[‡]Ernst Ruska-Centre for Microscopy and Spectroscopy with Electrons, Forschungszentrum Juelich GmbH, 52425 Juelich, Germany

[§]Department of Physics, Ruhr-University Bochum, 44780 Bochum, Germany

Supporting Information

ABSTRACT: Colloid-based chemical synthesis methods of bimetallic alloy nanoparticles (NPs) provide good monodispersity, yet generally show a strong variation of the resulting mean particle size with alloy composition. This severely compromises accurate correlation between composition of alloy particles and their size-dependent properties. To address this issue, a general CO adsorption-assisted capping ligand-free solvothermal synthesis method is reported which provides homogeneous bimetallic NPs with almost perfectly constant particle size over an unusually wide compositional range. Using Pt−Ni alloy NPs as an example, we show that variation of the reaction temperature between 160 and 240 °C allows for precise control of the resulting alloy particle bulk composition between 15 and 70 atomic % Ni, coupled with a constant mean particle size of ∼4 nm. The size-confining and Ni content-controlling role of CO during the nucleation and growth processes are investigated and discussed. Data suggest that size-dependent CO surface chemisorption and reversible Ni-carbonyl formation are key factors for the achievement of a constant particle size and temperature-controlled Ni content. To demonstrate the usefulness of the independent control of size and composition, size-deconvoluted relations between composition and electrocatalytic properties are established. Refining earlier reports, we uncover intrinsic monotonic relations between catalytic activity and initial Ni content, as expected from theoretical considerations.

Surface catalytic properties of nanometer-scale metal alloy materials are sensitively dependent on size and composition.[1] This is why an accurate intrinsic correlation of alloy particle size or composition with catalytic activity requires the availability of robust and preferably facile preparation techniques that provide independent control over particle size and composition.[2] Virtually all physical or wet-chemical alloy NP synthesis techniques reported to date fail to independently and precisely control size and composition and therefore often require empirical trial-and-error procedures to arrive at desired size or composition values.[3] Today, the most popular colloidal Synthesis for alloy nanoparticles is the "hot injection solvothermal polyol" method performed in presence of structure-directing organic capping ligands and high boiling point solvents.[3d,4−6] Polyol synthesis offers poor independent control over size and composition.[7] Composition control at constant size typically requires laborious trial-and-error optimization of the initial amounts of surfactant and precursor. The availablility of a one-pot, one-step method to control alloy NP composition and size independently is therefore desireable.

Here, a facile CO-assisted high-pressure synthesis of alloy NPs is reported and exemplified using the Pt−Ni bimetallic system. The synthesis is performed in dimethylforamide (DMF) at elevated pressures of CO, but without the use of any long-chain expensive organic capping ligands. We show that the reaction temperature alone can be used to precisely control the alloy particle composition from 15 to 70 at. % Ni without changing the initial precursor amount. Regardless of the Ni content, the resulting mean particle size is maintained at almost exactly 4 nm by virtue of the presence of CO. Based on our findings, we address and refine previously held views on the role of CO in such solvothermal synthetic environments. We provide evidence that CO molecules play a uniquely versatile role as a size-confining molecular adsorbate owing to its size-dependent chemisorption energy and coverage and as an effective Ni monomer concentration-controlling agent, while its previously suspected role of a reducing agent appears less relevant. The CO-assisted synthesis was applied to various Pt-M (M = Ni, Co) bimetallic systems. To demonstrate the usefulness of the size-confinement of nanocrystals over wide composition ranges, we utilize a set of 4 nm Pt−Ni particles and extract intrinsic activity-composition relations, which, unlike previous reports, suggest a simple linear relation between alloy composition and catalytic activity.

Size confinement. Pt−Ni alloy NPs were prepared by mixing $Pt(acac)_2$ and $Ni(acac)_2$ in identical initial molar ratios and subsequent reaction in a pressurized autoclave in the presence of 2 bar CO (over)pressure gas at four different reaction temperatures. Figure 1 shows the TEM images of four Pt−Ni alloy NPs with atomic compositions ranging from 15 to 70 at. % Ni (Figures 1A−D). Surprisingly, all four resulting Pt−Ni bimetallic nanocrystals showed identical diameters of about 4 nm

Received: December 13, 2013
Published: March 4, 2014

   dx.doi.org/10.1021/ja4124658 | J. Am. Chem. Soc. 2014, 136, 4813−4816

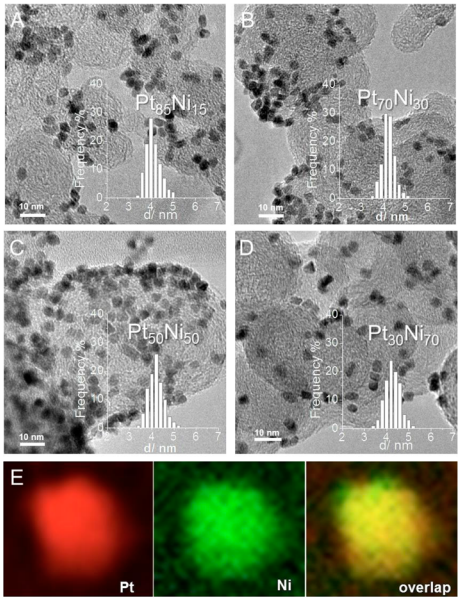

Figure 1. TEM images of Pt−Ni/C NPs. Insets show particle size distribution. (A) $Pt_{85}Ni_{15}$. (B) $Pt_{70}Ni_{30}$. (C) $Pt_{50}Ni_{50}$. (D) $Pt_{30}Ni_{70}$. (E) EELS elemental map of $Pt_{50}Ni_{50}$. Pt(red), Ni(green).

with a narrow size distribution (insets in Figure 1A−D). Most nanocrystals demonstrated an octahedral shape with a yield of ~60% (Figures 1A−D). The shape of the resulting particles was largely dependent on the metal precursor ligand employed, yet independent of CO pressure. To demonstrate the strong size-confining effect of the CO atmosphere on the NPs, Figure S1 displays and compares the temperature-dependent mean size of the resulting Pt−Ni alloy NPs in the absence of CO but otherwise identical conditions.[8] At ambient pressure (0 bar) and in the absence of CO, the resulting NP size ranged between 10 and 40 nm for reaction temperatures from 120 to 240 °C, evidencing a dramatic size-confining effect of the CO molecules. Additional reference measurements at CO partial pressures between 0.5 and 2 bar resulted in nanocrystals with larger mean sizes coupled to a lower degree of size confinement.

Composition control. While the particle size remained constant at all reaction temperatures at 2 bar CO, the bulk Ni content of the resulting 4 nm NPs followed the temperature in a nearly linear fashion. This made the reaction temperature a practical and powerful controlling parameter for the final composition of the bimetallic NPs. As shown in Figure 2A, when increasing the reaction temperature from 160 to 240 °C, the Pt−Ni alloy composition changed monotonically from

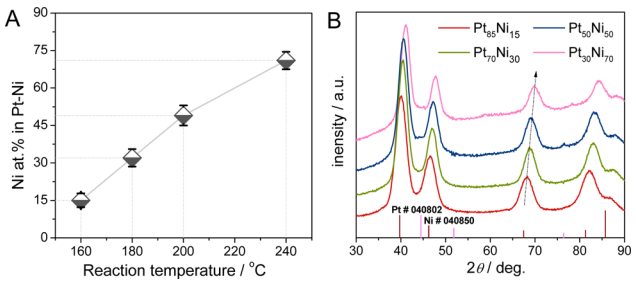

Figure 2. (A) Correlation between reaction temperature and Ni at. % in 4 nm Pt−Ni alloy NPs obtained at 2 bar CO. (B) XRD patterns of Pt−Ni NPs with different Ni/Pt compositional ratios.

$Pt_{85}Ni_{15}$ to $Pt_{30}Ni_{70}$, all at identical 4 nm diameter. This correlation between the reaction temperature and the Ni atomic fraction of the alloy particles in presence of CO provided a much more precise and convenient control of the Ni/Pt molar ratio of the NPs than was previously thought possible. The origin of this robust temperature-Ni at. % correlation is likely associated with the individual temperature-dependent chemical reduction rates of Pt and Ni.[9] While Pt appears to be reduced quantitatively at all reaction temperatures during the reaction time, elevated temperatures accelerate the reduction rate of Ni and increase the reduced amount of Ni relative to Pt. Control experiments at lower CO partial pressures (0−1 bar) showed drastically higher Ni atomic content of the Pt−Ni nanocrystals for any given temperature. For instance at 160 °C, 2 bar CO resulted in 4 nm nanocrystals with a Ni molar ratio x = 15 at. %, while at 0.5 bar CO this value rose to x = 20 at.%, while in the absence of CO, the Ni content was above 50 at. %. Since the Ni reduction rate is largely controlled by temperature and the concentration of free Ni monomers, our observations suggest an important, previously overlooked role of the CO gas molecules in terms of controlling the effective free Ni monomer concentration.

Evidently, solvated CO molecules display an interesting and versatile particle size-confining and composition-controlling effect under reaction conditions. From our control experiments we hypothesize a two-fold role of CO in this size-confining process. First, strong CO adsorption on Pt−Ni seeds and emerging nanocrystals (see "1" and "2" in Figure S2) leads to a gradual CO surface coverage build-up in accordance to earlier CO adsorption studies on PtNi NPs.[10] As a result of this, particle growth and particle ripening appear to be slowed down near a critical particle size of around 4 nm. This is the point where the CO adlayer has reached a critical coverage[11] that no longer allows further deposition of metal monomers nor the agglomeration of the nanocrystals. This is corroborated by the experimental observation that without any CO the Pt and Ni precursors form a dark metallic film on the glass lined autoclave as early as 160 °C, while in presence of 2 bar CO this undesired film deposition requires temperatures of over 250 °C, enabling the size-confined particle formation and stabilization over a much wider compositional range. Second, given the stoichiometric excess of CO as compared to Ni, we hypothesize that during the nucleation and growth of the NPs, CO molecules scavenge free metallic Ni monomers reversibly, forming nickel carbonyl species (Ni + 4 CO → $Ni(CO)_4$) ("4" in Figure S2). This process is well-known to occur at about 50 °C[12] and limits the effective concentration of free Ni monomers in the reaction mixture at low temperatures. At reaction temperatures above 180 °C, however, the Ni carbonyl complex becomes increasingly labile[12] and enables an increasingly higher effective free Ni concentration in the solvent, resulting in Ni-richer alloy NPs by combining with the increased reduction rate of Ni.

Earlier reports on the use of CO in the form of metal carbonyls suspected solvated CO to act as a key reducing[10c,13] and shape-controlling agent.[10c,14] In a previous report, CO was also found to affect the thickness of metal sheets.[15] Our data suggest that the elevated CO pressures explored under the present conditions do not affect the particle shape and do not noticeably accelerate the metal ion reduction process. The former can be plausibly rationalized by a loss of adsorption selectivity on crystal facets of specific surface orientation, because the CO interaction and coverage on different crystal facets may become nearly identical at the elevated CO pressures employed here. Furthermore, if CO were to accelerate the Ni reduction process, one would expect an

dx.doi.org/10.1021/ja4124658 | J. Am. Chem. Soc. 2014, 136, 4813−4816

increase in the Ni content with increasing CO pressure, in clear contrast with our experimental findings. Also, a simple control experiment performed at 160 °C in DMF employing $Ni(acac)_2$ in absence of the Pt precursor and CO gas confirmed an earlier report that $Ni(acac)_2$ can actually be reduced under these conditions.[16] Thus, we conclude that an additional reducing effect of solvated CO under the present conditions of temperatures of 160 to 240 °C is rather negligible and confirms earlier reports.[14c] We do note, however, that in DMF at temperatures below 160 °C the presence of Pt seeds was critical for the reduction of Ni ions, in line with findings in other solvents.[17]

We characterized the structure (Figure 2B), morphology (Figure S2C) and composition (Figure 1E) of the Pt–Ni NPs. Bragg reflections in Figure 2B revealed face-centered cubic crystal symmetries. Peak shifts toward higher 2-θ values with increasing Ni content (arrow) reflect near-linear lattice contractions (see Figure S3A).[18] Slight deviations from the ideal Vegard's law are likely due to minor XRD-invisible amorphous Ni oxide phases, as corroborated by XPS (see Figure S3B). The compositional distribution of Pt and Ni in the $Pt_{50}Ni_{50}$ catalyst was mapped by Cs-corrected scanning transmission electron microscopy complemented with electron energy loss spectroscopy (STEM-EELS) in Figure 1E.

To demonstrate the usefulness of our synthesis to obtain accurate size-deconvoluted correlations of catalytic activity and alloy composition, the oxygen reduction reaction (ORR) was chosen. When subject to a cyclic voltammetric pretreatment in acid electrolytes, Pt–Ni NPs in the 2–10 nm size range are known to undergo selective surface dissolution of Ni, thereby forming a Pt-enriched surface region surrounding a core region with a Ni content close to the initial value.[1c,7,19] Following earlier work on the effect of surface lattice strain on catalytic activity in Pt core shell particles,[1c,20] the Ni content in the particle core controls the surface lattice strain and also the catalytic activity. Higher Ni content in the core causes a smaller core lattice parameter and favors surface compressive strain and higher ORR activities.[21]

The four Pt–Ni alloy nanocatalysts were voltammetrically activated during 25 potential cycles in a 0.1 M $HClO_4$ electrolyte. This cycling leached out Ni atoms from the surface and resulted in the removal of about 60–66% of the initial Ni, as shown in Figure S4.[19a] The more Ni in the pristine catalyst, the more Ni was retained in the core region after voltammetric treatment (see Figure S5). Given the identical voltammetric activation protocol and initial particle size, while varying Ni content, this observation is quite plausible.[7] All four cyclic voltammograms (CVs) of the activated catalysts in Figure 3A exhibited the characteristic features of a Pt surface, while their ORR activities in Figure 3B display significant differences.

In contrast to earlier studies of ORR activity-composition trends of the Pt–Ni bimetallic NP system,[20,22] the trends in the Pt electrochemical surface area (ECSA)-normalized (Figure 3B) and in the Pt-mass normalized (Figure 3C) observed here suggest a strictly monotonic, nearly linear dependence of the activity on the initial Ni content of the alloy catalyst. This correlation would be expected from a surface lattice-strained core–shell catalyst particle,[1c,19a] as illustrated in the inset of Figure 4A. In fact, the Ni content in the NP core appears to follow their initial Ni value at a comparable Pt shell thickness. Earlier studies suggested ORR activity maxima for alloy particles at about 50–75 Ni at. %. However, these data were compromised by increasing NP sizes with increasing Ni content. Here, the most

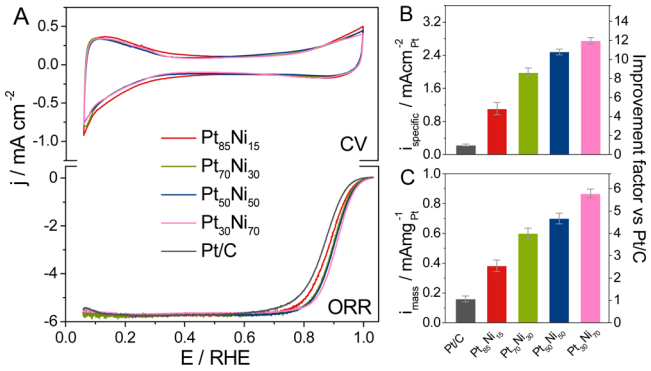

Figure 3. (A) CVs of the Pt–Ni NPs and their polarization curves for the ORR. (B) Specific Pt surface-area activities and (C) Pt-mass activities measured in 0.1 M $HClO_4$ with 1,600 rpm, 5 mVs^{-1} at 0.9 V with corresponding improvements factors versus the state-of-the-art commercial Pt catalyst.

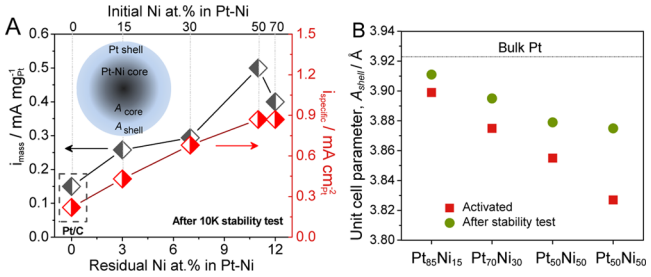

Figure 4. (A) Specific (red) and Pt mass (black) ORR activities as function of the Ni content for Pt–Ni NPs after a stability test involving 10,000 potential cycles. A commercial Pt/C catalyst was used as reference. Inset shows the model of an activated core–shell Pt–Ni NP. (B) Estimated unit cell parameters of Pt–Ni catalysts after electrochemical activation and stability testing. Dashed line: Pt bulk cell parameter.

active 4 nm $Pt_{30}Ni_{70}$ catalyst demonstrated a nearly 12 times higher surface-area normalized activity relative to a commercial pure Pt reference, which just falls short of the highest ever measured ORR activity of a 9 nm-sized octahedral Pt–Ni catalyst.[8]

The size-corrected activity-composition relation in Figure 3 implies that the initial Ni composition is actually a good descriptor for activity owing to the associated lattice strain.[1c] Given a monotonic relation between Ni dissolution and initial Ni content, a similar activity-composition relation should apply for the residual Ni content of the activated and long term tested catalysts, 25 and 10 000 cycles, respectively. Indeed, an experimental monotonic near-linear relationship between initial and residual Ni content was preserved (Figure S4 and S5). We also correlated the residual Ni contents with the catalytic activity (Figure 4A) and again revealed an essentially nearly linear monotonic relation for the core–shell particles.

The physical origin of the composition-activity relation is provided in Figure 4B, relating the unit cell parameter of the catalysts with the initial Ni content of the catalysts.[23] The difference in cell parameters of each catalyst and the dashed line represents a measure for the compressive Pt surface lattice strain, a structural descriptor for ORR activity.[1c,24] Figure 4 highlights the monotonic relation between the initial Ni content, Pt lattice strain, and ORR activity as expected from theoretical considerations.[1c,24]

dx.doi.org/10.1021/ja4124658 | J. Am. Chem. Soc. 2014, 136, 4813–4816

We also monitored the temporal evolution of the ORR activities (Figure S6), the cyclic voltammetry and associated ECSA (Figures S7 and S8), and the Ni content (Figures 4 and S4) of all catalysts during 10 000 potential cycles. As expected for Pt alloy core−shell catalysts, the Ni content and activity of all catalyst gradually decreased over extended catalytic test times. Nevertheless, unlike pure Pt NPs, the ECSA of the Pt−Ni alloy catalysts increased over the first 2,000 cycles and remained stable thereafter (Figure S7). These ECSA trajectories point to initial surface roughening due to Ni leaching followed by surface faceting during the electrochemical treatment rather than particle growth due to coalescence or ripening. This is consistent with the TEM micrographs of the tested alloy NPs in Figure S9, which document the morphological stability of the NPs.

To test the broader applicability of the CO-assisted size confinement of bimetallic alloy NPs, we demonstrated the feasibility of this method for the preparation of size-controlled Pt−Co NPs in Figure S10.

In summary, we present a novel CO-assisted, capping ligand-free synthesis for bimetallic alloy NPs at elevated pressures. What sets this method apart from conventional solvothermal techniques is its previously unachieved temperature-based composition control combined with the unique CO-adsorption based particle size confinement. We have exemplified the synthetic approach using the Pt−Ni system, however, it offers broader applicability to other Pt bimetallic systems and likely to alloy systems in general, provided sufficiently strong CO adsorption. We have shed light on the dual role of CO as size-confining and Ni content-controlling agent. We have demonstrated the usefulness of size-confinement for establishing accurate composition-property relationships, which otherwise would be compromised by size variations. We hope this study will spark more research into the use of gaseous surfactants in solvothermal synthesis.

■ ASSOCIATED CONTENT

Supporting Information

Experimental methods and analyses. This material is available free of charge via the Internet at http://pubs.acs.org.

■ AUTHOR INFORMATION

Corresponding Author

pstrasser@tu-berlin.de

Notes

The authors declare no competing financial interest.

■ ACKNOWLEDGMENTS

We thank Zelmi at TU Berlin, for support by SPP 1613 (DFG) and by BMBF (16N11929). B.R.C. acknowledges support by the Cluster of Excellence "RESOLV" funded by DFG (EXC 1069).

■ REFERENCES

(1) (a) Stamenkovic, V. R.; Fowler, B.; Mun, B. S.; Wang, G. F.; Ross, P. N.; Lucas, C. A.; Markovic, N. M. *Science* **2007**, *315*, 493. (b) Debe, M. K. *Nature* **2012**, *486*, 43. (c) Strasser, P.; Koh, S.; Anniyev, T.; Greeley, J.; More, K.; Yu, C. F.; Liu, Z. C.; Kaya, S.; Nordlund, D.; Ogasawara, H.; Toney, M. F.; Nilsson, A. *Nature Chem.* **2010**, *2*, 454.

(2) Cui, C.; Gan, L.; Heggen, M.; Rudi, S.; Strasser, P. *Nat. Mater.* **2013**, *12*, 765.

(3) (a) Wang, C.; Markovic, N. M.; Stamenkovic, V. R. *Acs Catalysis* **2012**, 891. (b) Somodi, F.; Werner, S.; Peng, Z. M.; Getsoian, A. B.; Mlinar, A. N.; Yeo, B. S.; Bell, A. T. *Langmuir* **2012**, *28*, 3345. (c) Shevchenko, E. V.; Talapin, D. V.; Rogach, A. L.; Kornowski, A.; Haase, M.; Weller, H. *J. Am. Chem. Soc.* **2002**, *124*, 11480. (d) Shevchenko, E. V.; Talapin, D. V.; Schnablegger, H.; Kornowski, A.; Festin, Ö.; Svedlindh, P.; Haase, M.; Weller, H. *J. Am. Chem. Soc.* **2003**, *125*, 9090.

(4) Kwon, S. G.; Hyeon, T. *Small* **2011**, *7*, 2685.

(5) (a) Zhang, S.; Guo, S. J.; Zhu, H. Y.; Su, D.; Sun, S. H. *J. Am. Chem. Soc.* **2012**, *134*, 5060. (b) Zhu, H. Y.; Zhang, S.; Guo, S. J.; Su, D.; Sun, S. H. *J. Am. Chem. Soc.* **2013**, *135*, 7130. (c) Guo, S.; Zhang, S.; Sun, S. *Angew. Chem., Int. Ed.* **2013**, *52*, 8526.

(6) Li, D. G.; Wang, C.; Tripkovic, D.; Sun, S. H.; Markovic, N. M.; Stamenkovic, V. R. *Acs Catalysis* **2012**, *2*, 1358.

(7) Snyder, J.; McCue, I.; Livi, K.; Erlebacher, J. *J. Am. Chem. Soc.* **2012**, *134*, 8633.

(8) Cui, C.; Gan, L.; Li, H.-H.; Yu, S.-H.; Heggen, M.; Strasser, P. *Nano Lett.* **2012**, *12*, 5885.

(9) (a) Burda, C.; Chen, X. B.; Narayanan, R.; El-Sayed, M. A. *Chem. Rev.* **2005**, *105*, 1025. (b) Oezaslan, M.; Hasché, F.; Strasser, P. *Chem. Mater.* **2011**, *23*, 2159.

(10) (a) Cui, C.; Ahmadi, M.; Behafarid, F.; Gan, L.; Neumann, M.; Heggen, M.; Cuenya, B. R.; Strasser, P. *Faraday Disc.* **2013**, *162*, 91. (b) Kirstein, W.; Krüger, B.; Thieme, F. *Surf. Sci.* **1986**, *176*, 505. (c) Wu, B.; Zheng, N.; Fu, G. *Chem. Commun.* **2011**, *47*, 1039.

(11) (a) Mayrhofer, K. J. J.; Juhart, V.; Hartl, K.; Hanzlik, M.; Arenz, M. *Angew. Chem., Int. Ed.* **2009**, *48*, 3529. (b) Acs CatalysisAndersson, K. J.; Calle-Vallejo, F.; Rossmeisl, J.; Chorkendorff, L. *J. Am. Chem. Soc.* **2009**, *131*, 2404. (c) Pantförder, A.; Skonieczny, J.; Janssen, E.; Meister, G.; Goldmann, A.; Varga, P. *Surf. Sci.* **1995**, *331*−333, 824. (d) Eiswirth, M.; Burger, J.; Strasser, P.; Ertl, G. *J. Phys. Chem.* **1996**, *100*, 19118.

(12) Lascelles, K.; Morgan, L. G.; Nicholls, D.; Beyersmann, D. *Nickel Compounds*; Wiley-VCH: Weinheim, 2005.

(13) Wu, J. B.; Gross, A.; Yang, H. *Nano Lett.* **2011**, *11*, 798.

(14) (a) Li, H.; Chen, G.; Yang, H.; Wang, X.; Liang, J.; Liu, P.; Chen, M.; Zheng, N. *Angew. Chem., Int. Ed.* **2013**, *52*, 8368. (b) Zhang, J.; Yang, H.; Fang, J.; Zou, S. *Nano Lett.* **2010**, *10*, 638. (c) Choi, S. I.; Xie, S.; Shao, M.; Odell, J. H.; Lu, N.; Peng, H.-C.; Protsailo, L.; Guerrero, S.; Park, J.; Xia, X.; Wang, J.; Kim, M. J.; Xia, Y. *Nano Lett.* **2013**, *13*, 3240. (d) Chen, G. X.; Tan, Y. M.; Wu, B. H.; Fu, G.; Zheng, N. F. *Chem. Commun.* **2012**, *48*, 2758. (e) Chen, G.; Yang, H.; Wu, B.; Zheng, Y.; Zheng, N. *Dalton Trans.* **2013**, *42*, 12699. (f) Kang, Y.; Ye, X.; Murray, C. B. *Angew. Chem., Int. Ed.* **2010**, *49*, 6156.

(15) Huang, X. Q.; Tang, S. H.; Mu, X. L.; Dai, Y.; Chen, G. X.; Zhou, Z. Y.; Ruan, F. X.; Yang, Z. L.; Zheng, N. F. *Nat. Nanotechnol.* **2011**, *6*, 28.

(16) Zhang, Z.; Chen, X.; Zhang, X.; Shi, C. *Solid State Commun.* **2006**, *139*, 403.

(17) Wang, D.; Peng, Q.; Li, Y. *Nano Res* **2010**, *3*, 574.

(18) Travitsky, N.; Ripenbein, T.; Golodnitsky, D.; Rosenberg, Y.; Burshtein, L.; Peled, E. *J. Power Sources* **2006**, *161*, 782.

(19) (a) Strasser, P. *Rev. Chem. Eng.* **2009**, *25*, 255. (b) Oezaslan, M.; Heggen, M.; Strasser, P. *J. Am. Chem. Soc.* **2011**, *134*, 514.

(20) Gan, L.; Heggen, M.; Rudi, S.; Strasser, P. *Nano Lett.* **2012**, *12*, 5423−5430.

(21) Norskov, J. K.; Rossmeisl, J.; Logadottir, A.; Lindqvist, L.; Kitchin, J. R.; Bligaard, T.; Jonsson, H. *J. Phys. Chem. B* **2004**, *108*, 17886.

(22) (a) Wang, C.; Chi, M.; Wang, G.; van der Vliet, D.; Li, D.; More, K.; Wang, H.-H.; Schlueter, J. A.; Markovic, N. M.; Stamenkovic, V. R. *Adv. Funct. Mater.* **2011**, *21*, 147. (b) Liu, Y.; Hangarter, C. M.; Bertocci, U.; Moffat, T. P. *J. Phys. Chem. C* **2012**, *116*, 7848.

(23) (a) Stephens, I. E. L.; Bondarenko, A. S.; Perez-Alonso, F. J.; Calle-Vallejo, F.; Bech, L.; Johansson, T. P.; Jepsen, A. K.; Frydendal, R.; Knudsen, B. P.; Rossmeisl, J.; Chorkendorff, I. *J. Am. Chem. Soc.* **2011**, *133*, 5485. (b) Stamenkovic, V.; Schmidt, T. J.; Ross, P. N.; Markovic, N. M. *J. Phys. Chem. B* **2002**, *106*, 11970.

(24) Mavrikakis, M.; Hammer, B.; Norskov, J. K. *Phys. Rev. Lett.* **1998**, *81*, 2819.